



# Micro-milling mechanism and surface roughness of high volume fraction SiCp/Al composites

Po Jin<sup>1</sup> · Qi Gao<sup>1</sup> · Quanzhao Wang<sup>2</sup> · Wenbo Li<sup>1</sup>

Received: 25 January 2021 / Accepted: 16 April 2021 / Published online: 3 May 2021  
© The Author(s), under exclusive licence to Springer-Verlag London Ltd., part of Springer Nature 2021

## Abstract

In this paper, a finite element simulation model of diamond tool milling SiCp/Al composites was established. The cutting stress, stress distribution and material removal mechanism of the SiC-reinforced material were studied. At the same time, the correctness of the finite element simulation was verified by a micro-milling experiment. The results show that the main particle removal methods include pulling out, crushing and pressing in and that the particle removal methods are different when the tool is cutting at different positions. With increasing cutting speed, the surface defects of the material are reduced and the surface quality is improved. The main surface defects in the milling process are voids, microcracks, scratches and pits. Through the optimization of cutting parameters, it is found that the milling depth has the greatest effect on the surface roughness, the spindle speed has the second greatest effect, and the feed rate has the least effect. The surface roughness of the machined workpiece is 0.238  $\mu\text{m}$  when the process parameters have been optimized.

**Keywords** SiCp/Al composite · Micro-milling · Milling mechanism · Surface roughness · Orthogonal experiment

## 1 Introduction

Because of the increasing requirements for material properties in aerospace, automotive and optical precision instruments, SiC particle-reinforced aluminium matrix composites (SiCp/Al) have attracted increasing attention due to their excellent properties [1]. The SiCp/Al composites have excellent comprehensive properties, such as high specific strength and modulus and high temperature resistance. The SiCp/Al components are mainly used in satellite bearings, aircraft engines and inertial navigation systems [2]. Due to the urgent need for SiCp/Al composites in various projects, the processing technology of SiCp/Al composites has been widely studied by scholars [3].

Song et al. [4, 5] found that, with increasing SiC particle volume fraction, the yield strength and tensile strength

increased, while the elongation decreased. Subsequently, Wang et al. [6] established a two-dimensional (2D) finite element simulation model to study the milling process of SiCp/Al matrix composite materials. He found that the main causes of surface defects were extrusion, pull-out and crushing of particles. Teng et al. [7] established a 2D finite element simulation model considering the cutting-edge radius and analysed the interaction between the cutter and particles and the process of chip formation. The distribution of cutting stress and strain in the workpiece under the influence of different milling depths was studied. Niu et al. [8] carried out machining experiments with polycrystalline diamond (PCD) tools on a high-precision micro-milling machine and analysed the surface roughness, morphology, texture and defects of the workpiece. They also chose the best process parameters. Pramanik et al. [9] performed milling on nanoparticle-reinforced aluminium matrix composites. The results show that the surface roughness of the workpiece increases with increasing feeding speed. The surface roughness of the workpiece decreases with increasing feed per tooth at a higher feed rate (100–140 m/min). Liu et al. [10] established a force prediction model for SiCp/Al composites. He found that the maximum milling force increases with increasing feed per tooth and milling depth. Dabade et al. [11] studied two kinds of

✉ Qi Gao  
qqonline@163.com

<sup>1</sup> School of Mechanical Engineering and Automation, Liaoning University of Technology, Jinzhou 121001, China

<sup>2</sup> Institute of Metal Research, Chinese Academy of Science, Shenyang 110016, China

SiCp composites with a volume fraction of 10%. The effects of the feed rate and milling depth on the cutting force, surface roughness and preheating temperature were revealed. Ge et al. [12] studied the wear condition, chip formation and surface generation of the cutter when the low-body SiCp/2009Al composite material was processed at ultrahigh speed. Liu et al. [13, 14] conducted an experimental study on micro-milling of 45% SiCp/Al composites. They found that the surface roughness first decreased and then increased with increasing feed. Wang et al. [15] simulated the high-speed milling process of SiCp/Al6063 composites with a high volume fraction. The interactions among the matrix, particles and tools during cutting were studied. The cutting mechanism of the material was also revealed. Wang et al. [16] studied the milling process of SiCp/Al composites with a high volume fraction and small particle size. The effects of milling speed, feed rate and particle size on tool wear were revealed. Quan et al. [17] studied the hardness and residual stress of SiCp/Al composites during processing. The results show that the residual stress on the surface of coarse-grained reinforced composites may be released due to structural defects. However, the residual stress on the surface of the composite reinforced with fine grains tends to compress. Bian et al. [18] conducted precision milling research on SiCp/Al composites with a high volume fraction and large granularity. The cutting mechanism and wear characteristics of the SiCp/Al composites were revealed. Kumar et al. [19] fabricated SiC- and B<sub>4</sub>C-reinforced aluminium composites with three different components using the agitation casting technique. Experiments were carried out on these materials with different machining parameters, and the most influential milling parameters were found. Teng et al. [20] investigated the cutting mechanism of two SiCp/Al composites with different particle sizes. It was found that the nanoscale particles remained intact during the cutting process without breaking, which may produce a continuous chip. However, micron-sized particles are prone to fracture and tend to produce discontinuous chips. Compared with micron-sized materials, nanometre-sized materials can achieve better surface quality and fewer defects. Han et al. [21] used an experimental apparatus to study the factors affecting tool wear and the quality of machined surfaces. The result shows that the cutting-edge strength with chamfered edges is greatly improved. The increase in feed and milling depth leads to an increase and decrease in machining surface roughness.

Due to the strengthening effect of silicon carbide particles in the material, SiCp/Al composites have excellent properties. At the same time, the surface quality of the processed material is difficult to control, which is typical for a refractory material [22]. Micro-milling is an important machining method in the field of mechanical processing and has many advantages, such as high machining accuracy and low machining cost.

Therefore, micro-milling technology is applied to the processing of composite materials to realize the flexible and precise processing of composite parts [23, 24].

The removal characteristics of composites are different from those of conventional machining. Both the size effect of plastic material and the removal of brittle material affect the surface formation of composite materials. In this paper, finite element simulation and micro-milling experiments are combined to study the material milling mechanism and surface defect formation mechanism of SiCp/Al composites in microcutting. The influence of the spindle speed, feed rate and milling depth on surface quality is analysed. Furthermore, the optimization of the combination of process parameters is carried out to further improve the surface quality of the material and promote its industrial application.

## 2 Simulation analysis based on the particle random distribution model

SiCp/Al composites are a two-phase heterogeneous material composed of an aluminium alloy matrix and micron-grade silicon carbide particles. Because the characteristics of a two-phase materials are different, a model of particle random distribution is constructed, and the simulation experiment is carried out.

### 2.1 Establishment of a random particle distribution model

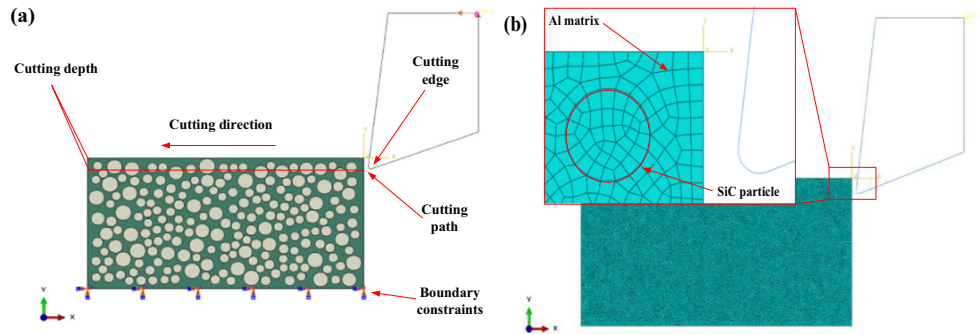
A cutting simulation model of SiCp/Al composites with different particle size distributions is established. The 3D micro-milling model is simplified to a 2D orthogonal simulation experiment. The particle volume fraction of the composites is 60%. The particle diameter is mainly 20  $\mu\text{m}$  and 60  $\mu\text{m}$ . The average particle size is 40  $\mu\text{m}$ , and the matrix material is Al2024. It is assumed that the particle shape is circular and that the particles are randomly distributed in the matrix without overlapping.

This model and simulation were carried out in the Abaqus software, and the dimensions used were length (mm), mass (t) and time (s). The free mesh is used in the simulation, and the global mesh density of the SiCp/Al composite model is 5  $\mu\text{m}$ . The grid unit adopts CPE4RT, and the Dynamic, Temp-Disp and Explicit Step analysis steps are used. The cutting simulation model and meshing are shown in Fig. 1.

### 2.2 Material characteristics and failure criteria

The matrix of the composite is Al2024, and the reinforcement is SiC particles. The elastic phase of the material is mainly determined by the elastic modulus and Poisson's ratio. The parameters are shown in Table 1.

**Fig. 1** Schematic diagram of a cutting model. (a) Cutting simulation model. (b) Meshing



Aluminium is a typical plastic material. The Johnson-Cook (J-C) model is used to characterize its plastic deformation stage [25], and it is often characterized as follows:

$$\sigma = \left( A + B\bar{\epsilon}^{pn} \right) \left( 1 + C \ln \frac{\dot{\bar{\epsilon}}}{\dot{\bar{\epsilon}}_0} \right) \left[ 1 - \left( \frac{T - T_0}{T_{melt} - T_0} \right)^m \right] \quad (1)$$

where  $\sigma$  is the flow stress (MPa);  $\epsilon$  is the effective plastic strain;  $\bar{\epsilon}$  is the effective plastic strain rate;  $\dot{\bar{\epsilon}}_0$  is the reference plastic strain rate;  $T$  is the environment temperature ( $^{\circ}\text{C}$ );  $T_m$  is the melting point temperature of the material;  $A$  is the yield stress of the material (MPa);  $B$  is the work hardening parameters of the material (MPa);  $C$  is the strain rate enhancement index;  $m$  is the temperature change rate index; and  $n$  is the strain hardening index.

The Johnson-Cook fracture criterion and damage parameter  $D$  were used to judge the material removal.  $D$  was set to be 1, and the unit was separated and removed. The expression is

$$D = \sum \frac{\Delta\epsilon}{\epsilon^f} \quad (2)$$

where  $\epsilon^f$  is the failure strain and  $\Delta\epsilon$  is the effective plastic strain increment under an increase in the load unit.

Using the J-C fracture criterion [26], the calculation formula for equivalent plastic strain is

$$\epsilon^f = \left[ d_1 + d_2 \exp \left( d_3 \frac{\delta_m}{\delta} \right) \right] \left( 1 + d_4 \ln \frac{\dot{\epsilon}}{\dot{\epsilon}_0} \right) \left[ 1 + d_5 \left( \frac{T - T_r}{T_m - T_r} \right) \right] \quad (3)$$

where  $\epsilon^f$  is the equivalent plastic strain;  $\delta_m$  is the average value of positive pressure (MPa);  $\delta$  is the effective stress (MPa); and

**Table 1** Material parameters of Al2024 and SiC

| Material  | Matrix: Al2024 | Particles: SiC |
|---|----------------|----------------|
| Density ( $\text{g}/\text{cm}^3$ )              | 2.77           | 3.13           |
| Elastic modulus (GPa)                           | 73             | 427.5          |
| Poisson's ratio                                 | 0.33           | 0.14           |
| Thermal conductivity ( $\text{W}/(\text{mk})$ ) | 190            | 81             |
| Specific heat ( $\text{J}/(\text{kgK})$ )       | 875            | 427            |

$d_1 - d_5$  are the material failure parameters. Table 2 shows the J-C model and J-C fracture model parameters of the 2024 aluminium alloy.

The PCD tool is set as an analytical rigid body in the simulation. The cutting-edge radius is  $10 \mu\text{m}$ , the rake angle is  $7^{\circ}$ , and the relief angle is  $20^{\circ}$ . The contact mode is face-to-face contact, and the Coulomb friction model is adopted, with a friction coefficient of 0.35. The bottom of the matrix and the upper right part of the tool are constrained by the boundary.

### 2.3 Criteria for chip separation

The characteristics of the aluminium matrix also adopt the J-C and J-C fracture models [28], adopt brittleness removal criteria for SiC particles and select a tensile stress standard to judge, and its characterization is as follows:

$$\max (\delta_1, \delta_2, \delta_3) = \delta_0 \quad (4)$$

where  $\delta_1, \delta_2, \delta_3$  is the principal stress (MPa) and  $\delta_0$  is the crushing stress of the SiC material (MPa).

In the failure criterion of brittle materials, the standard model of energy is used to measure the cracking and crack expansion of silicon carbide. The crack displacement during failure can be expressed by

**Table 2** Some parameters of matrix J-C model and J-C fracture model [27]

|                              |        |
|------------------------------|--------|
| $A$ (MPa)                    | 369    |
| $B$ (MPa)                    | 684    |
| $C$                          | 0.0083 |
| $m$                          | 1.7    |
| $n$                          | 0.73   |
| $d_1$                        | 0.112  |
| $d_2$                        | 0.123  |
| $d_3$                        | 1.5    |
| $d_4$                        | 0.007  |
| $d_5$                        | 0      |
| $T_m$ ( $^{\circ}\text{C}$ ) | 502    |
| $T_r$ ( $^{\circ}\text{C}$ ) | 20     |

**Table 3** Parameters of material brittleness removal [28, 29]

| $\delta_0$ | $G_f^l$ | $p$ | $e_{max}^{ck}$ |
|------------|---------|-----|----------------|
| 1500       | 30      | 1   | 0.001          |

$$u_{n0} = 2G_f^l / \delta_m^l \tag{5}$$

where  $u_{n0}$  is the nominal displacement ( $\mu\text{m}$ );  $G_f^l$  is the mode I fracture energy ( $\text{J}/\text{m}^2$ ); and  $\delta_m^l$  is the critical stress of the mode I fracture (MPa).

The stress retention model is used to describe crack propagation due to shear stress. The shear modulus  $G_c$  after cracking can be calculated by the following formula:

$$G_c = \left(1 - \frac{e_{mn}^{ck}}{e_{max}^{ck}}\right)^p G \tag{6}$$

where  $p$  and  $e_{max}^{ck}$  are material parameters;  $G$  is the shear modulus of the material (MPa); and  $e_{mn}^{ck}$  is the crack propagation strain. The brittle fracture parameters of the SiC material standards are shown in Table 3.

### 2.4 The relationship between the experiment and simulation

In the experiment, the maximum milling depth is  $50 \mu\text{m}$ , which is very small compared to the cutter diameter of  $1000 \mu\text{m}$ , as shown in Fig. 2. In this case, the effect of the helix angle on chip formation and cutting force is negligible. Therefore, the machining process of 3D micro-milling is simplified to a 2D micro-orthogonal machining process. It is assumed that the uncut chip thickness in the cutting process is the same as that set in the simulation.

### 2.5 Analysis of the cutting mechanism and results

In the simulation, the cutting speed is set to  $37.68 \text{ m}/\text{min}$ , which is equivalent to a spindle speed of  $12,000 \text{ r}/\text{min}$ , and the cutting thickness is  $40 \mu\text{m}$ . After the simulation, the particle removal and surface defects are analysed, and it is found

that the removal forms of cutting particles are also different at different positions, as shown in Fig. 3.

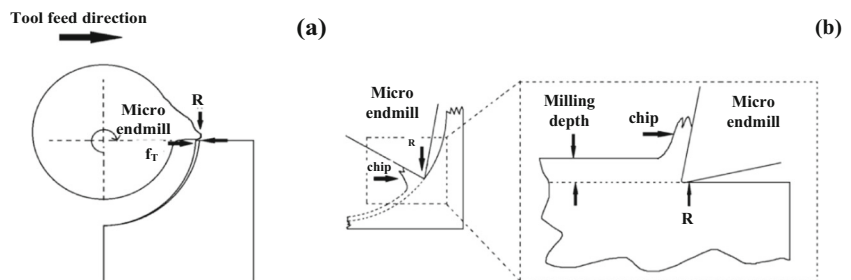
It can be seen from Fig. 3 that, when cutting SiCp/Al composites, the main removal forms of particles are peeling, shedding, crushing and pressing. Because the particle size and position are randomly selected when the model is established, the removal of particles is also different when the tool is cutting different positions of the particles.

Figure 3(c) and (d) show the upper part of the particle being cut by the PCD tool. The interface between the particles and the aluminium matrix is destroyed. The part above the point where the particles contact the tip is removed and the following part is pressed into the matrix. The tool first cuts the aluminium matrix, and the aluminium matrix deforms plastically. As the cutting progresses, the tool tip approaches the particle gradually, the constraint between the particle and the matrix fails, and the aluminium matrix is removed plastically. When the cutting stress is greater than the limit value of the particle material strength, the particle experiences brittle deformation. With the process of cutting, the amount of deformation expands, the upper part of the particle is peeled off, and the surface of the workpiece produces cracks and pits.

In Fig. 3(a) and (b), the situation near the middle position of the particle cut by the PCD tool is shown. In the cutting tool, most of the particle interface fails, and a few particles are directly pressed into the matrix. When the tool cuts the middle part of the particle, the aluminium matrix is extruded by the particle and the tool to produce plastic deformation. The constraint failure of the aluminium matrix transforms into the cutting process of the silicon carbide particle. When the cutting stress is greater than the limit value of the particle material strength, the brittle deformation of the particle is removed.

Figure 3(d)–(f) show the PCD tool cutting the lower half and bottom of the particle. At this point, the interface completely fails, and the particles are directly pulled out. Under the cutting tool, the particles squeeze each other and this also causes the particles to break and be removed. When the tool cuts the lower part of the particle, the constraint gradually fails when the tool tip contacts the chip. The cutting stress is greater than the particle material strength limit, the interface is completely ineffective, the lower half of the particle is crushed, most of the particle is pulled out, and the machining surface produces a large pit. When the tool cuts the

**Fig. 2** (a) Two-dimensional milling process diagram when the tool rotates  $180^\circ$ . (b) Relationship between 2D milling process and orthogonal machining process



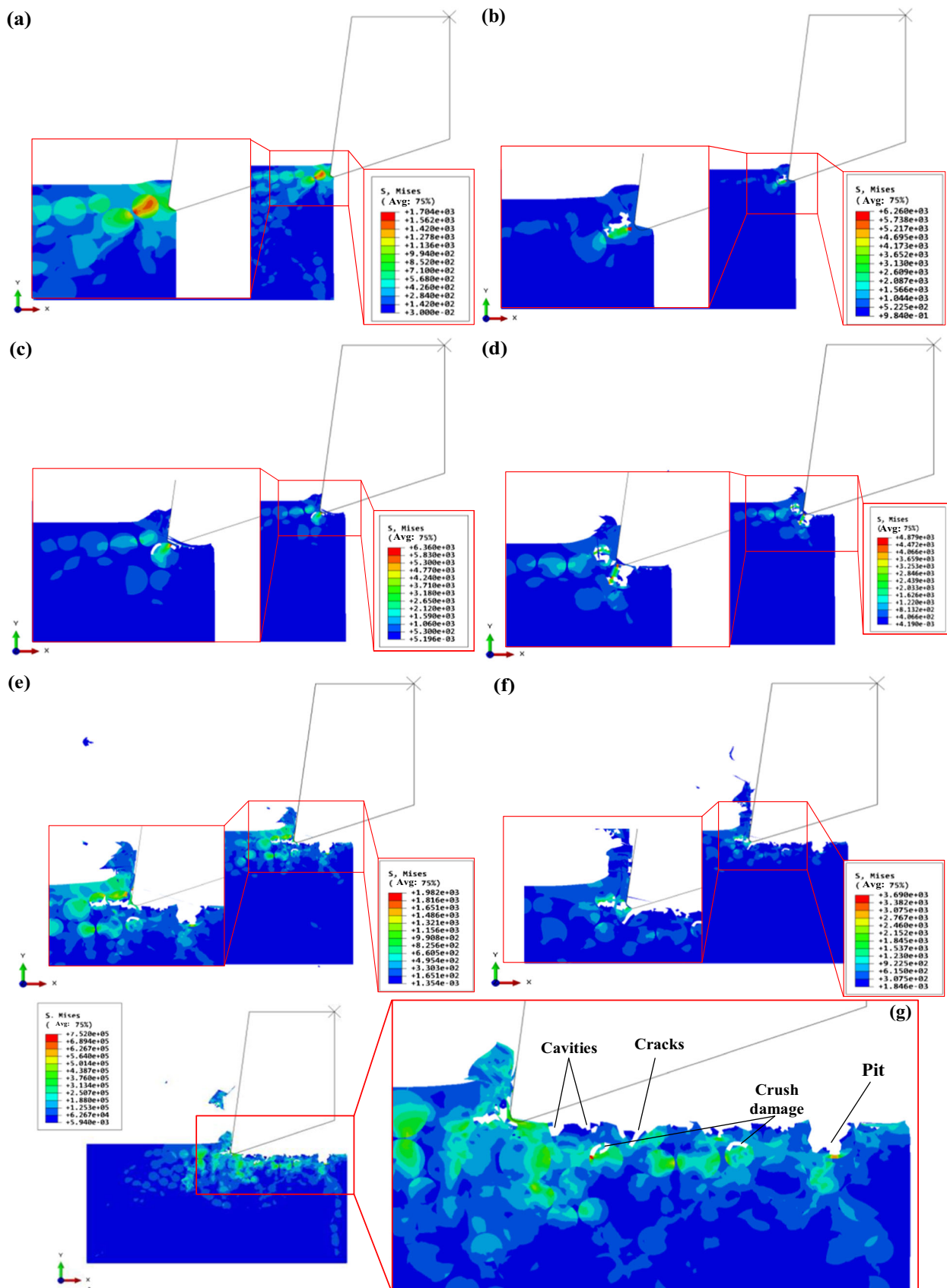


Fig. 3 Removal mode and surface morphology of particles in simulation. (a)–(f)  $V_c = 37.68$  m/min,  $h = 40$   $\mu$ m particle removal mode. (g)  $V_c = 37.68$  m/min,  $h = 40$   $\mu$ m surface morphology



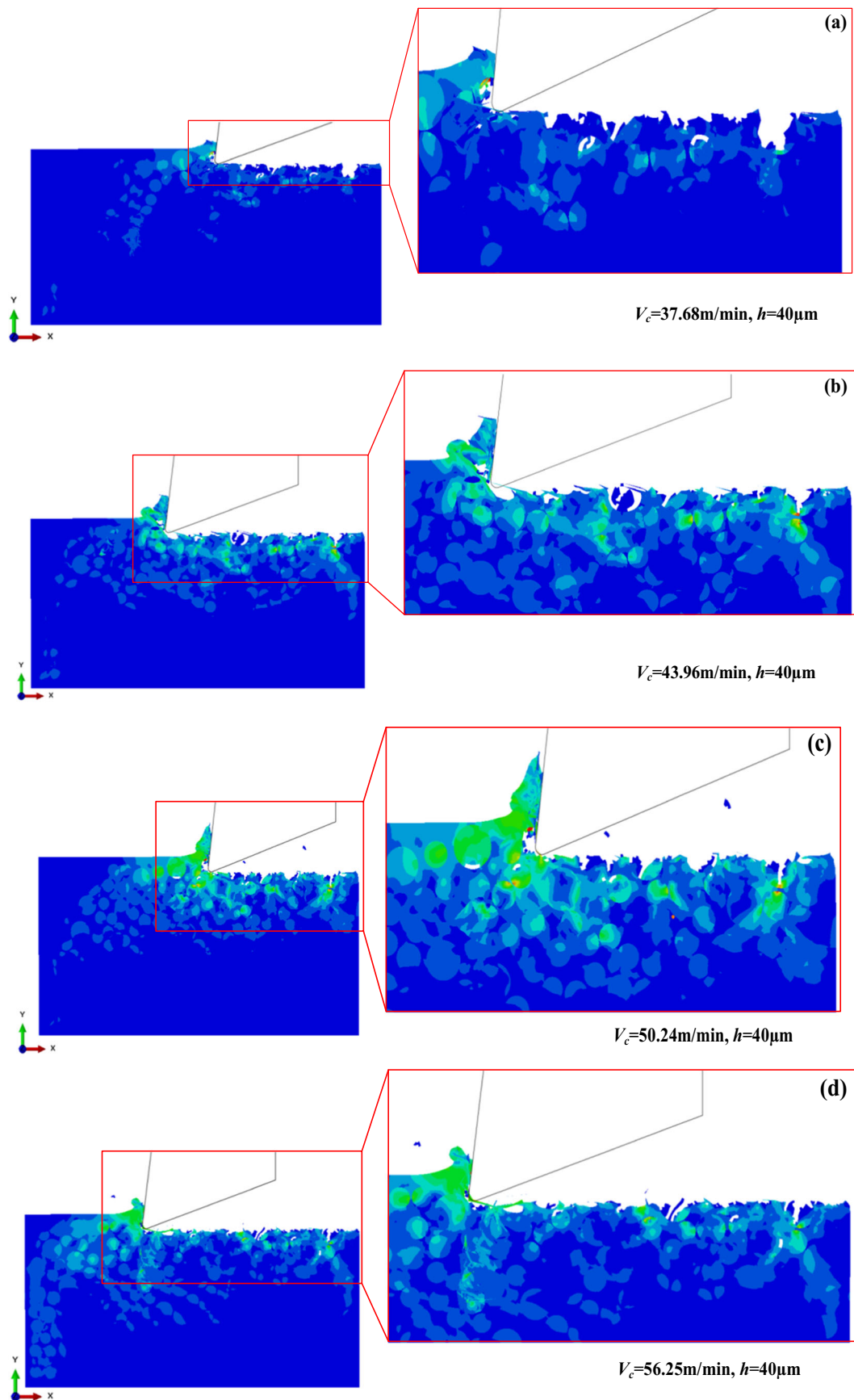
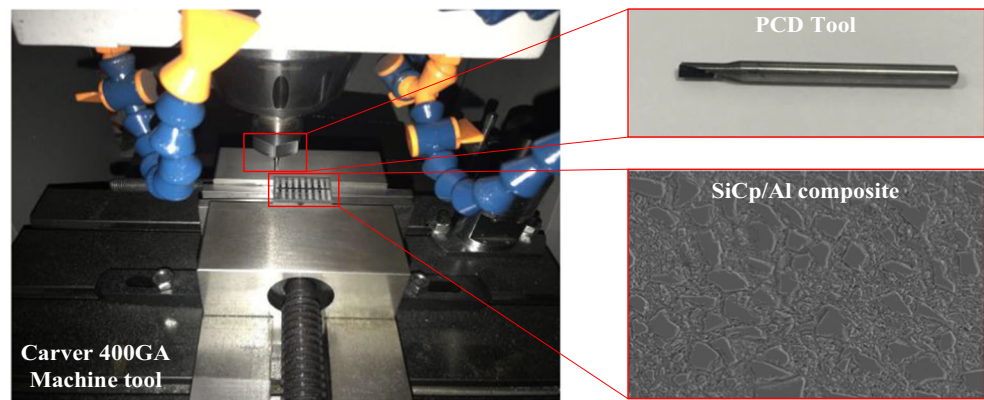


Fig. 4 Morphology of SiCp/2024Al composite micromachined surface

Fig. 5 Experimental site



bottom of the particle, the contact surface near the bottom of the particle and matrix leads to constraint failure cuts. With the progress of cutting, the particles are completely pulled out, and the surface quality is better.

It can be seen from Fig. 3g that, in the cutting process, the stress concentration area is mainly the plane where the matrix and particles contact, and the irregular stress distribution area mainly appears in the position area where the tool, particles and matrix materials interact. It can be concluded that stress concentration and irregular stress distribution are the main reasons for particle breakage, peeling, shedding, extrusion and surface defects.

The particle removal and surface defects after the simulation are shown in Fig. 4.

As shown in Fig. 5, with increasing cutting speed, the cracks and defects of the particles decrease, and the material surface quality improves. The main reason is that the cutting stress in the system increases with increasing cutting speed, so the strain rate increases. According to the J-C failure criterion, the increase in stress and strain rate makes the matrix easy to remove. For SiC particles, the increase in cutting speed results in a decrease in the time taken to cut the particles. Compared with low cutting speeds, the tool interacts with particles for a shorter time, and the stress transfer time is shorter, reducing crack growth and defect formation. Therefore, there are fewer surface defects in the material, and the surface morphology is smoother during high-speed cutting.

### 3 Experimental study on micro-milling

#### 3.1 The experimental scheme

The experiment mainly studies and analyses the surface defects formed by a PCD end mill milling a groove when processing particle-reinforced aluminium matrix composite SiCp/Al and the influence of milling dosage on the surface quality. The material used in the experiment was a SiCp/Al composite material composed of Al2024 aluminium alloy and SiC particles. The volume fraction of particles is 60%. The particle part is mainly composed of 20  $\mu\text{m}$  and 60  $\mu\text{m}$  particles with an average size of 40  $\mu\text{m}$ . A diamond end mill is selected as the experimental tool. The tool diameter is 1 mm, the edge radius is 10  $\mu\text{m}$ , the rake angle is 7°, and the relief angle is 20°.

This experiment was carried out on the 3D micro-milling machine platform as shown in Fig. 5. The surface roughness value of the material cuttings was measured by a real colour scanning microscope. The surface micromorphology of the material cuttings was observed by a Zeiss SIGMA 500 field emission scanning electron microscope, and the experimental equipment is shown in Fig. 6.

This micro-milling experiment mainly studies the influence of process parameters on surface roughness. The processing parameters used in the milling test are shown in Table 4.

Through orthogonal testing, the degree of influence of each parameter is determined so that it can be optimized. According to the three process parameters spindle speed, feed rate and

Fig. 6 Experimental measurement equipment. (a) True colour confocal microscope. (b) Zeiss SIGMA 500 field emission scanning electron microscope

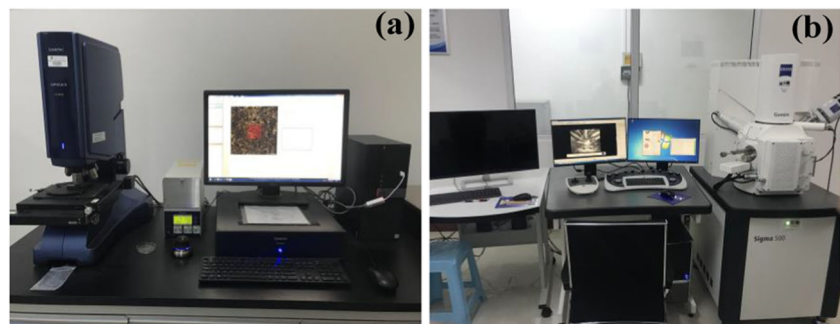


**Table 4** Parameter selection of orthogonal test

| Spindle speed (r/min) | Feed rate (mm/min) | Milling depth ( $\mu\text{m}$ ) |
|-----------------------|--------------------|---------------------------------|
| 12,000                | 6                  | 20                              |
| 14,000                | 8                  | 30                              |
| 16,000                | 10                 | 40                              |
| 18,000                | 12                 | 50                              |

milling depth, an orthogonal experiment of three factors and four levels was designed, and the influence of the interaction was ignored. Process parameters and their levels are shown in Table 5.

### 3.2 Analysis of the experimental results

Due to the existence of reinforced silicon carbide particles in particle-reinforced aluminium matrix composites, the effects of the micromorphology, formation rule and cutting parameters on the machined surface quality of the composites are different from those of the one-way material of the workpiece.

The micromorphology of the milling surface of particle-reinforced aluminium matrix composites was detected by real colour scanning microscopy, and four groups of experiments with obvious and representative surface micromorphology characteristics were selected for analysis. The three-dimensional features of the surface topography are shown in Fig. 7.

The three-dimensional features according to the observed surface topography are shown in Fig. 7. The machining surface in Fig. 7(c) is relatively smooth; that is, when the spindle speed is 16,000 r/min, the feed rate is 6 mm/min and the milling depth is 40  $\mu\text{m}$ , and the surface morphology of the material is relatively good.  $R_a$  is 0.385  $\mu\text{m}$ .

There are two main reasons for this: (1) The uncut chip thickness is slightly larger than the minimum cutting thickness of the aluminium matrix, and the removal effect of the aluminium matrix is better. (2) The milling volume of particles is small, and there are few broken particles, so the milling force is small and the amplitude of the spindle is small, which makes the surface quality better. The feed per tooth increases, the milling volume of the aluminium matrix and particles

**Table 5** Process parameters and their levels

| Parameters                            | Level |        |        |        |        |
|---------------------------------------|-------|--------|--------|--------|--------|
|                                       |       | 1      | 2      | 3      | 4      |
| Spindle speed $N$ (r/min)             | A     | 12,000 | 14,000 | 16,000 | 18,000 |
| Feed rate $V_f$ (mm/min)              | B     | 6      | 8      | 10     | 12     |
| Milling depth $a_p$ ( $\mu\text{m}$ ) | C     | 20     | 30     | 40     | 50     |

increases with time, the material size effect is weakened, and most of the particles are broken and removed when the spindle speed remains unchanged and the feed rate increases. The broken tiny particles scratch the surface under the extrusion of the tool. The formation of small cavities and scratches is shown in Fig. 7(a), (b) and (d), and the surface defects increase. In addition, many scratches and small cavities were also found on the surface of the material by scanning electron microscopy (SEM), as shown in Fig. 10(a).

In Fig. 7(a) and (b), there are large pits and cracks. The reason for this phenomenon is that the milling volume of the aluminium matrix and particles increases with time, which increases the milling force and aggravates the vibration of the spindle. In the experiment, the size of the material particles was large (20–60  $\mu\text{m}$ ). When the milling depth or feed per tooth is too large, it leads to cracks and cavities caused by particle extrusion and crushing, as well as pits caused by the particle pulling out.

The micromorphology of the milling surface of the particle-reinforced aluminium matrix composite was detected by a Zeiss SIGMA 500 field emission scanning electron microscope, and the surface defects of the material are shown in Fig. 8.

The surface roughness values corresponding to the four sets of cutting parameters (a), (b), (c) and (d) are shown in Fig. 9.

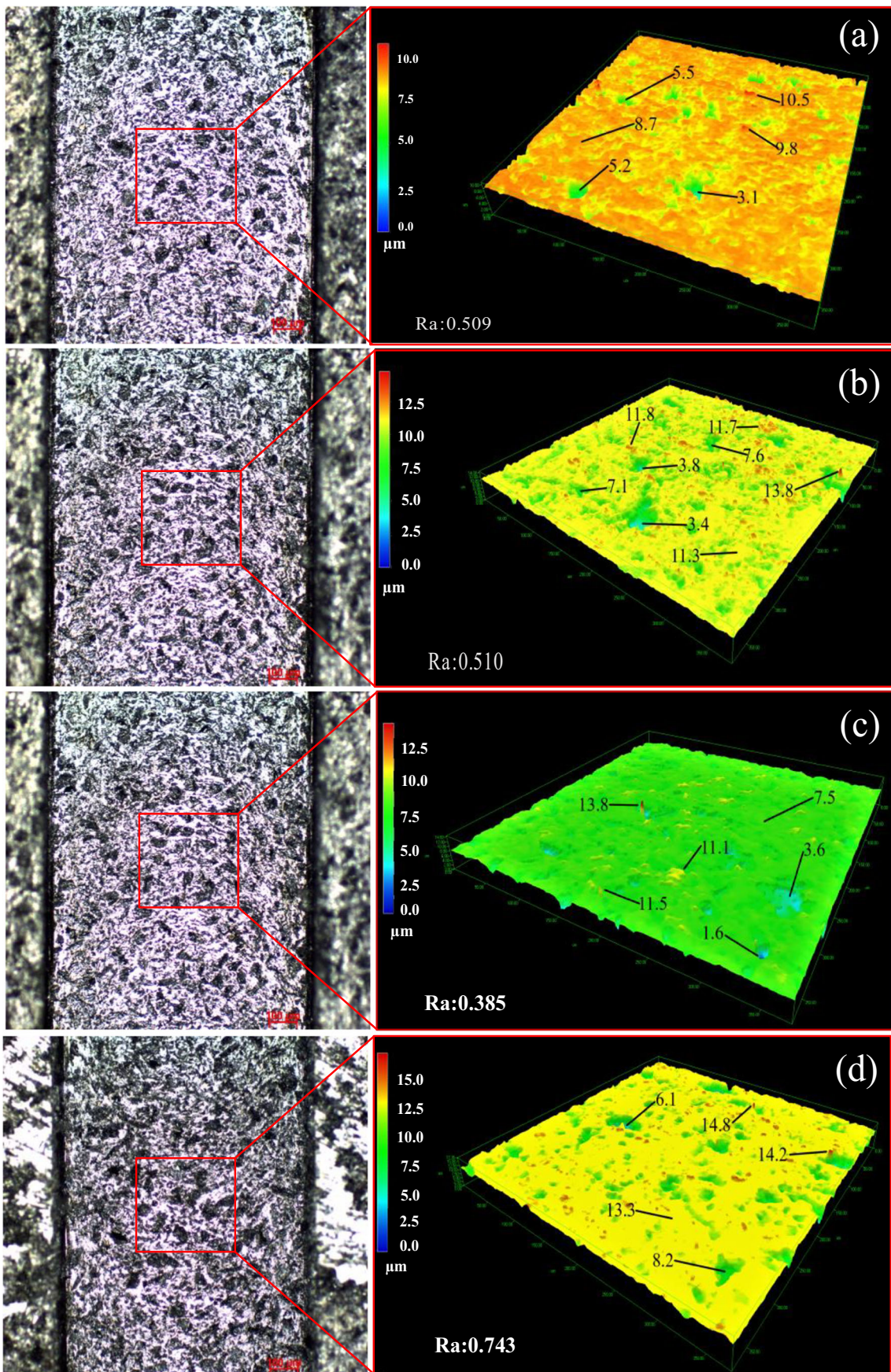
The detection energy spectrum of the surface of the processed material is shown in Fig. 10. The spindle speed is 12,000 r/min, the feed rate is 0.006 m/min, and the milling depth is 40  $\mu\text{m}$ .

Figure 8 clearly shows the cracks and cavities caused by particles being crushed in the milling process of the composite materials, the scratches caused by crushed particles being rolled and the cavities caused by particles being pulled out. These defects are clearly shown in the finite element simulation model, and the experimental pictures verify the correctness of the finite element simulation model to a certain extent.

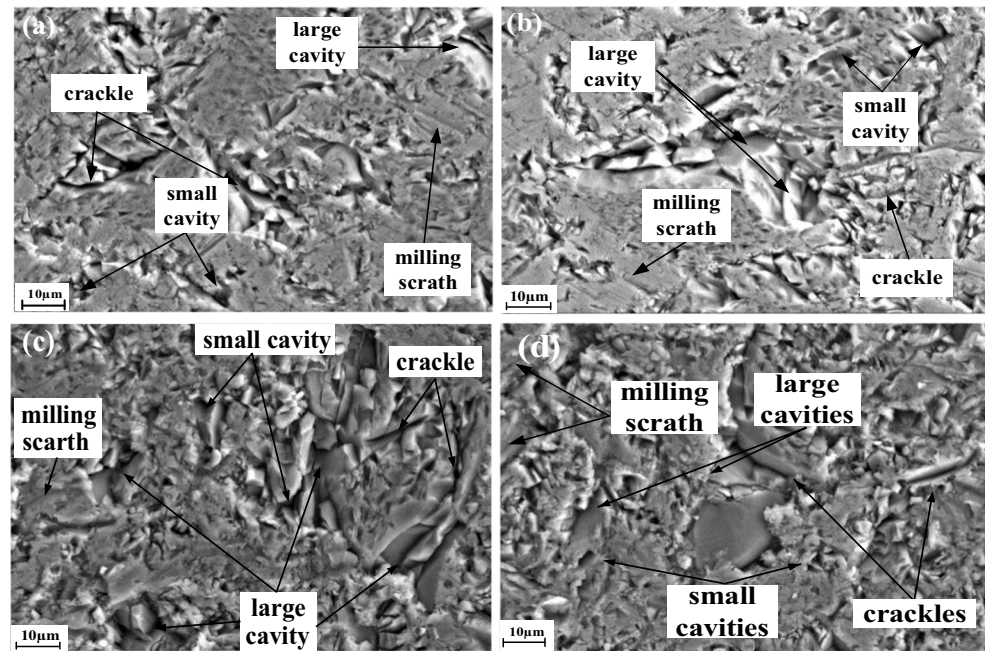
By combining Figs. 8 and 9, it can be found that, when the feed per tooth increases, the surface defects of the processed material first increase rapidly, and then decrease rapidly and then increase slowly; and the surface quality first increases rapidly, and then decreases rapidly and then increases slowly. During the milling process, the milling depth remained unchanged, and with the increase in tooth feeding, the surface roughness parameter  $R_a$  decreased rapidly after increasing rapidly, which shows that when  $f_z$  is 0.5  $\mu\text{m}$ , the phenomenon of ploughing occurs and the  $R_a$  value is likely to increase. The

**Fig. 7** Three-dimensional feature map of surface morphology. (a)  $N=14,000$  r/min,  $V_f=0.012$  m/min,  $a_p=50$   $\mu\text{m}$ . (b)  $N=14,000$  r/min,  $V_f=0.01$  m/min,  $a_p=50$   $\mu\text{m}$ . (c)  $N=16,000$  r/min,  $V_f=0.006$  m/min,  $a_p=40$   $\mu\text{m}$ . (d)  $N=18,000$  r/min,  $V_f=0.012$  m/min,  $a_p=20$   $\mu\text{m}$





**Fig. 8** Material surface defect detection with the same milling depth and different feeds per tooth. (a)  $f_z = 0.5 \mu\text{m}$ ,  $a_p = 40 \mu\text{m}$ . (b)  $f_z = 0.571 \mu\text{m}$ ,  $a_p = 40 \mu\text{m}$ . (c)  $f_z = 0.625 \mu\text{m}$ ,  $a_p = 40 \mu\text{m}$ . (d)  $f_z = 0.667 \mu\text{m}$ ,  $a_p = 40 \mu\text{m}$



increase in feed rate per tooth leads to an increase in milling volume per unit time. At the same time, the milling force and tool vibration increase, which increases the number of surface defects. The falling particles roll and slide along with the tool on the machined surface, which causes scratches on the workpiece surface and worsen the surface quality. With the increase of each tooth feed, the milling force increases, the friction is serious, the temperature rises rapidly, and the residual

aluminium matrix on the surface of the workpiece melts and binds to the material surface, resulting in a decrease of surface roughness.

According to the detection results in Fig. 10(a), point b contains 89.20% Si and 3.68% Al, point c contains 68.85.20% Si and 5.19% Al, and point a contains 67.23% Si and 16.59% Al. According to the detection results in Fig. 10(b), point b is a SiC particle, indicating that the particle

**Fig. 9** Surface roughness value corresponding to (a), (b), (c) and (d)

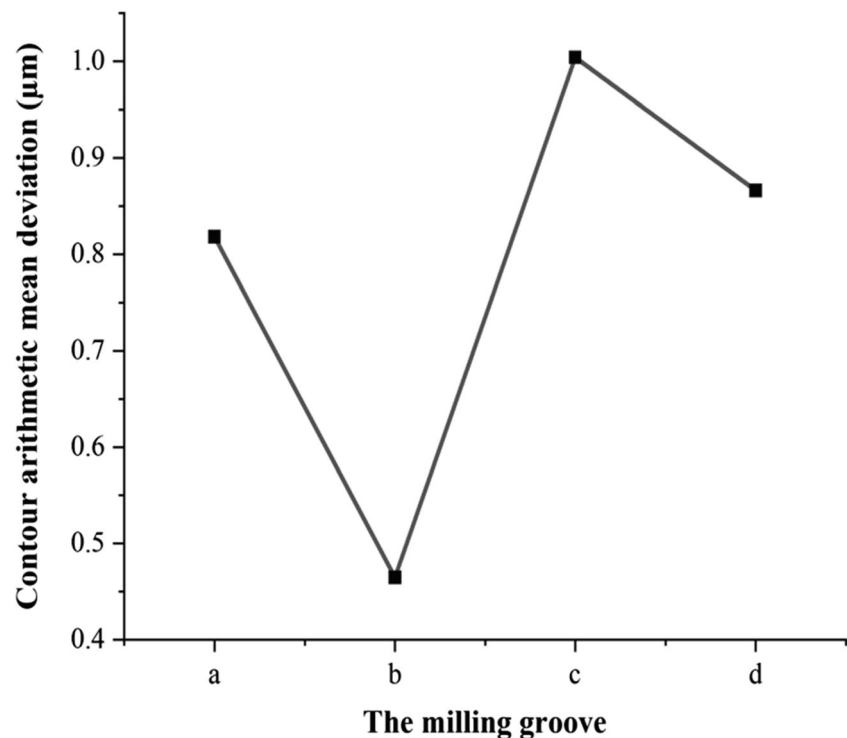
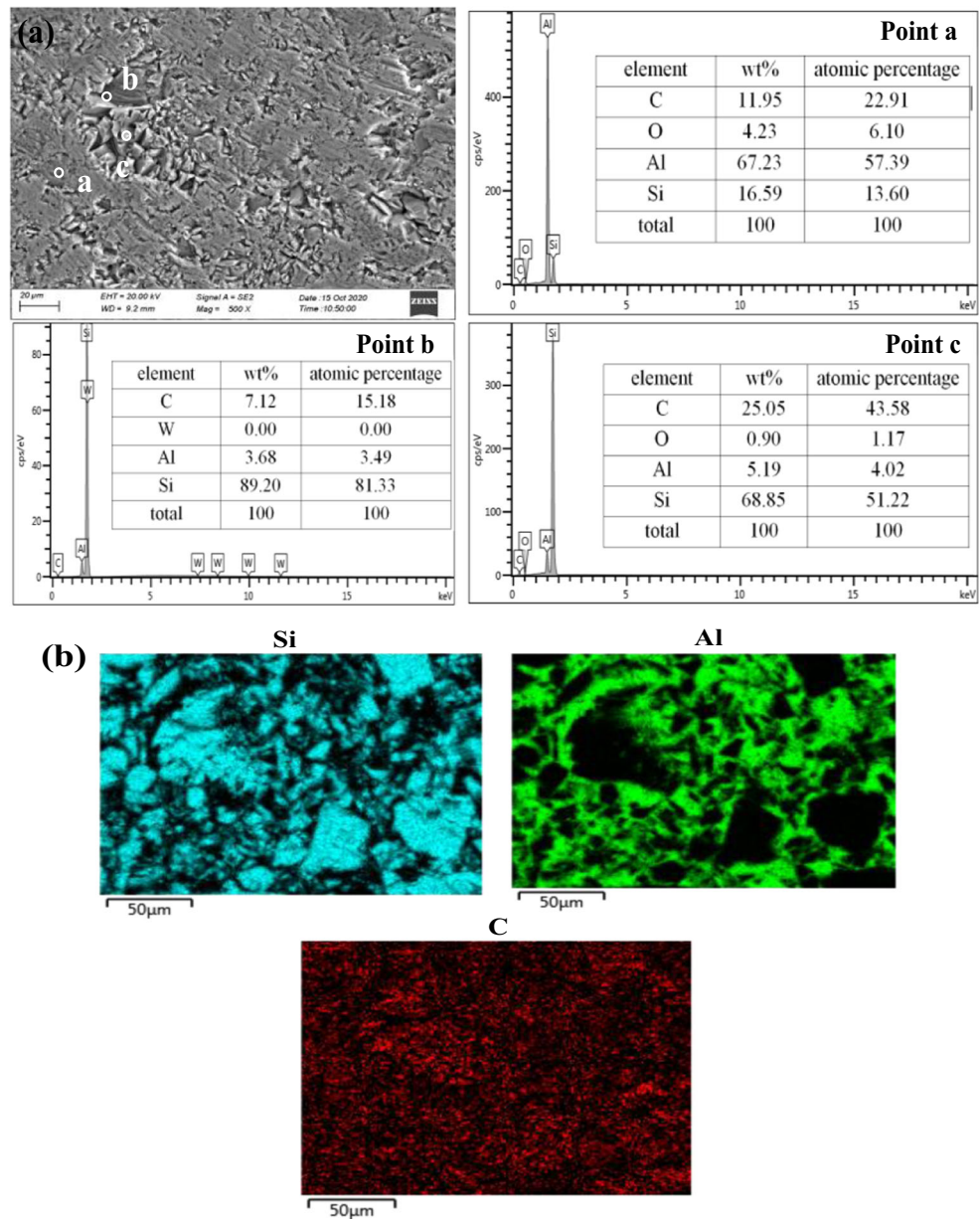




**Fig. 10** Composite material surface material detection diagram. (a) Surface material point detection. (b) Surface detection surface scanning



is broken and pulled out from the part, and point b is the hole caused by the particle being pulled out. Combined with Fig. 10(b), it can be found that the aluminium matrix is attached to the SiC particles.

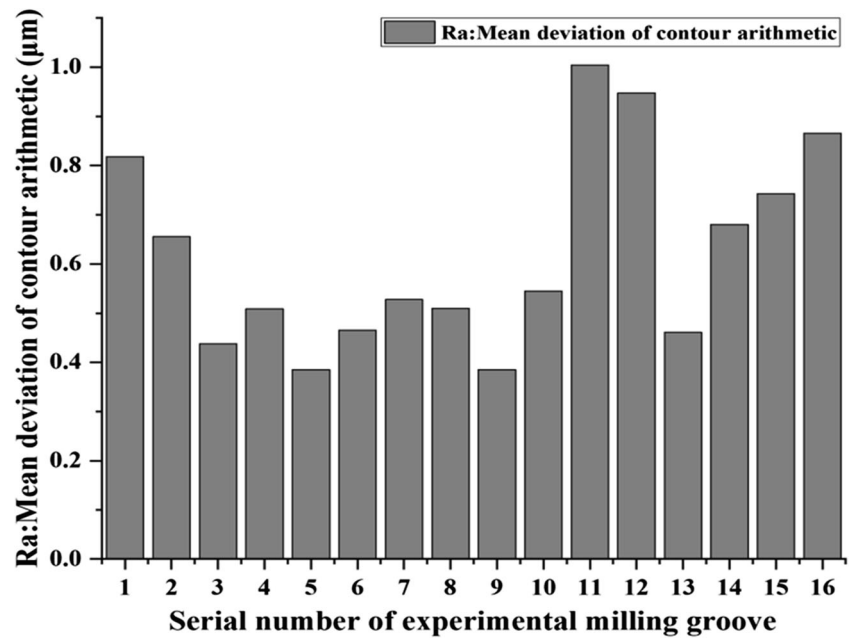
Due to the incomplete removal of the chip generated during milling, a small amount of residue is melted at high temperature and remains on the workpiece surface. As the milling progresses, the friction heat generation increases; as a result, more of the aluminium matrix remains on the processing surface after melting, surface defects of materials can be repaired, and the surface quality can be improved.

#### 4 Orthogonal experimental analysis and parameter optimization

The evaluation method of surface roughness selected in this paper is the centreline method, which is mainly used for  $R_a$  evaluation.  $R_a$  represents the arithmetic mean of the absolute value of the distance of contour offset from the undulating centreline along the measured direction within the sampling length. Its calculation formula:

$$R_a = \frac{1}{n} \sum_{i=1}^n |y_i| \tag{7}$$

**Fig. 11** Measurement results of surface roughness of milling groove



where  $y_i$  represents the distance between the point on the contour line and the centreline in the measured direction.

The measurement results of the orthogonal experiment are shown in Fig. 11.

According to the measurement results, the range analysis of the arithmetic mean deviation of the contour is shown in Table 6.

Table 6 shows that milling depth has the greatest influence on surface roughness, followed by spindle speed and feed rate. The optimum combination of surface roughness parameters is as follows: shaft speed 14,000 r/min, feed rate 6 mm/min and milling depth 40 μm. The surface morphology of the SiCp/Al composites obtained by milling with these parameters is shown in Fig. 12.

Through the optimization of cut parameters, it is found that, when using a diamond end mill with a smaller diameter and blade diameter to process a large particle high volume silicon carbide metal composite, the degree of influence of each parameter is very small, indicating that the surface consistency of the workpiece is high. The surface roughness is 0.238 μm.

## 5 Conclusion

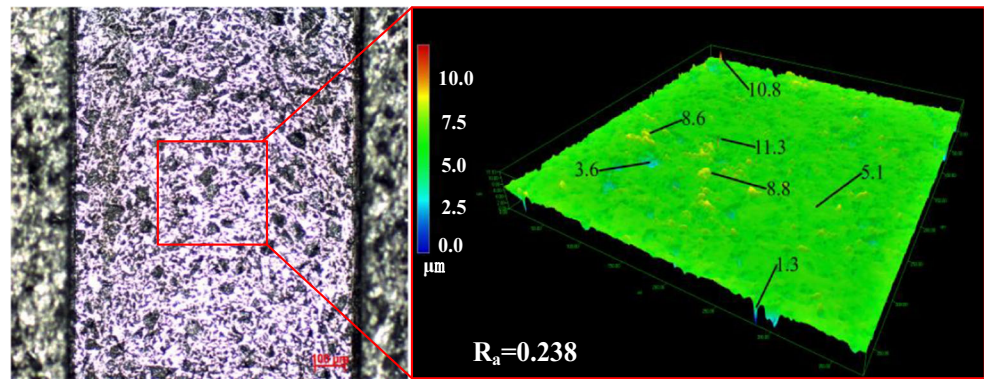
From the simulation and experimental results, the following conclusions were obtained:

**Table 6** Analysis of surface roughness range

| Experiment number           | Spindle speed A (r/min)                   | Feed rate B (μm) | Milling depth C (μm) |
|-----------------------------|---|------------------|----------------------|
| $K_1$                       | 2.42                                      | 2.049            | 3.097                |
| $K_2$                       | 1.888                                     | 2.345            | 2.787                |
| $K_3$                       | 2.882                                     | 2.713            | 2.013                |
| $K_4$                       | 2.75                                      | 2.833            | 2.043                |
| $k_1$                       | 0.605                                     | 0.51225          | 0.77425              |
| $k_2$                       | 0.472                                     | 0.58625          | 0.69675              |
| $k_3$                       | 0.7025                                    | 0.67825          | 0.50325              |
| $k_4$                       | 0.6875                                    | 0.70825          | 0.5015               |
| Range                       | 0.2305                                    | 0.196            | 0.27275              |
| Primary and secondary order | Milling depth > Spindle speed > Feed rate |                  |                      |
| Optimal levels              | $A_2$                                     | $B_1$            | $C_3$                |
| Optimal combination         | $A_2B_1C_3$                               |                  |                      |



**Fig. 12** Surface 3D morphology characteristics of  $N = 14,000$  r/min,  $V_f = 0.006$  m/min and  $a_p = 50$   $\mu\text{m}$



In the micro-milling process of silicon aluminium carbide composite materials, the main forms of particle removal are peeling, shedding, crushing and pressing, and the removal of particles at different positions of the cutting tool is also different.

In the process of milling, keeping the spindle speed and feed rate unchanged and increasing the milling depth eventually lead to a decrease in the surface quality of the material being machined. Keeping the milling depth and feed rate constant and increasing the spindle speed result in better surface quality of the material to be machined.

Through the optimization of cutting parameters, it can be found that the milling depth has the greatest influence on the surface roughness  $R_a$ , followed by the spindle speed and the feed rate. The optimal process parameters of surface roughness are as follows: spindle speed 14,000 r/min, feed rate 6 mm/min and milling depth 40  $\mu\text{m}$ . The surface roughness is 0.238  $\mu\text{m}$ .

The increase in each tooth feed leads to a rapid rise in temperature in the processing process, which leads to the melting and adhesion of the aluminium metal remaining on the workpiece surface. This situation improves the quality of the machined surface.

Through the optimization of milling parameters, it is found that the milling depth has the greatest influence on the surface roughness, followed by the spindle speed and feed rate when the PCD tool with a small cutting-edge radius is used to mill the SiCp/Al composite with large particles.

**Notation**  $N$ , Spindle speed;  $V_f$ , Feed rate;  $a_p$ , Milling depth;  $V_c$ , Cutting speed;  $h$ , Cutting thickness

**Author contribution** The finite element simulation experiment of micro-milling of SiCp/Al composites was established. The milling process of SiCp/Al composites with high volume fraction and large grain size was studied. The distribution of stress and strain of SiC-reinforced particles and the material removal mechanism were analysed. The influence degree of each influencing factor on surface roughness was determined.

**Funding** This work was supported by the National Natural Science Foundation of China (No. 51775100) and the Doctoral Start-up Fund of Liaoning Province (2019-BS-123).

**Data availability** The data used to support the findings of this study are available from the corresponding author upon request.

## Declarations

**Ethics approval** This research project has been approved by the Ethics Committee of Liaoning University of Technology. The authors state that the research was conducted according to ethical standard.

**Consent to participate** I solemnly declare that the paper “Micro-Milling Mechanism and Surface Roughness of High Volume Fraction SiCp/Al Composites” presented by us is the result of our research. This paper does not contain any work published or written by any other individual or group, except for the content specifically noted and cited in the paper. I fully realize that the legal consequences of this statement shall be borne by me.

**Consent for publication** The author confirms that the work described has not been published before; that it is not under consideration for publication elsewhere; that its publication has been approved by all co-authors, if any; that its publication has been approved by the responsible authorities at the institution where the work is carried out.

The author agrees to publication in the journal indicated below and also to the publication of the article in English by Springer in Springer’s corresponding English-language journal. The copyright to the English-language article is transferred to Springer effective if and when the article is accepted for publication. The author warrants that his/her contribution is original and that he/she has full power to make this grant. The author signs for and accepts responsibility for releasing this material on behalf of any and all co-authors. The copyright transfer covers the exclusive right to reproduce and distribute the article, including reprints, translations, photographic reproductions, microform, electronic form or any other reproductions of similar nature. After submission of the agreement signed by the corresponding author, changes of authorship or in the order of the authors listed will not be accepted by Springer. Journal: The International Journal of Advanced Manufacturing Technology, chemical samples. Names of all contributing authors: Po Jin, Qi Gao, Quanzhao Wang and Wenbo Li.

**Conflict of interest** The authors declare no competing interests.

## References

- Bhattacharyya JJ, Mitra R (2012) Effect of hot rolling temperature and thermal cycling on creep and damage behavior of powder metallurgy processed Al–SiC particulate composite. *Mater Sci Eng A-Struct* 557(NOV.15):92–105
- Chan KC, Cheung CF, Ramesh MV, Lee WB, To S (2001) A theoretical and experimental investigation of surface generation in diamond turning of an Al6061/SiCp metal matrix composite. *Int J Mech Sci* 43(9):2047–2068
- Durante S, Rutelli G, Rabezzana F (1997) Aluminum-based MMC machining with diamond-coated cutting tools. *Surf Coat Technol* 94(none):632–640
- Song M (2009) Effects of volume fraction of SiC particles on mechanical properties of SiC/Al composites. *Trans Nonferrous Metal Soc* 19(6):1400–1404
- Cui Y, Wang LF, Ren JY (2008) Multi-functional SiC/Al composites for aerospace applications. *Chin J Aeronaut* 21(6):578–584
- Wang T, Xie LJ, Wang XB (2015) Simulation study on defect formation mechanism of the machined surface in milling of high volume fraction SiCp/Al composite. *Int J Adv Manuf Technol* 79(5–8):1185–1194
- Teng XY, Huo DH, Chen WQ, Wong E, Zheng L, Shyha I (2018) Finite element modelling on cutting mechanism of nano Mg/SiC metal matrix composites considering cutting edge radius. *J Manuf Process* 32(APR.):116–126
- Niu ZC, Cheng K (2019) An experimental investigation on surface generation in ultraprecision machining of particle reinforced metal matrix composites. *Int J Adv Manuf Technol* 105(8):4499–4507
- Pramanik A, Basak AK, Dong Y, Subramaniam S, Littlefair G (2018) Milling of nanoparticles reinforced Al-based metal matrix composites. *J Compos Sci* 2(1):13
- Liu JW, Cheng K, Ding H, Chen SJ (2020) An analytical model for force prediction in micromilling silicon carbide particle-reinforced aluminum matrix composites. *Proc Inst Mech Eng B J Eng* 234(10):095440542092341
- Dabade UA, Jadhav MR (2016) Experimental study of surface integrity of Al/SiC particulate metal–matrix composites in hot machining. *Proc CIRP* 41:914–919
- Ge YF, Xu JH, Fu YC (2011) Experimental study on high-speed milling of SiCp/Al composites. *J Mater Process Technol* 291–294:725–731
- Liu JW, Cheng K, Ding CSJ, Zhao L (2018) An investigation of the influence of phases' removal ways on surface quality in micro milling SiCp/Al composites. *Proc CIRP* 71:59–64
- Liu JW, Cheng K, Ding H, Chen SJ, Zhao L (2019) Realization of ductile regime machining in micro-milling SiCp/Al composites and selection of cutting parameters. *Proc Inst Mech Eng C J Mech* 233(12):4336–4347
- Wang BB, Xie LJ, Chen XL, Wang XB (2016) The milling simulation and experimental research on high volume fraction of SiCp/Al. *Int J Adv Manuf Technol* 82(5–8):809–816
- Wang T, Xie LJ, Wang XB, Ding ZW (2015) PCD tool performance in high-speed milling of high volume fraction SiCp/Al composites. *Int J Adv Manuf Technol* 78:1445–1453
- Quan YM, Ye BY (2003) The effect of machining on the surface properties of SiC/Al composites. *J Mater Process Technol* 138(1–3):464–467
- Bian R, He N, Li L, Zhan ZB, Wu Q, Shi ZY (2013) Precision milling of high volume fraction SiCp/Al composites with mono-crystalline diamond end mill. *Int J Adv Manuf Technol* 71(1–4):411–419
- Bhuvanesh Kumar M, Parameshwaran R, Deepandurai K, Senthil SM (2020) Influence of milling parameters on surface roughness of Al–SiC–B4C composites. *Trans Indian Inst Metals* 73(5)
- Teng XY, Chen WQ, Huo DH, Shyha I, Lin C (2018) Comparison of cutting mechanism when machining micro and nano-particles reinforced SiC/Al metal matrix composites. *Compos Stroct* 203(NOV.):636–647
- Han JJ, Hao XQ, Li L, Wu Q, He N (2017) Milling of high volume fraction SiCp/Al composites using PCD tools with different structures of tool edges and grain sizes. *Int J Adv Manuf Technol* 92:1875–1882
- Ramesh MV, Chan KC, Lee WB, Cheung CF (2001) Finite-element analysis of diamond turning of aluminium matrix composites. *Compos Sci Technol* 61(10):1449–1456
- Chavoshi SZ, Goel S, Morantz P (2017) Current trends and future of sequential micro-machining processes on a single machine tool. *Mater Des* 127(aug.):37–53
- Liu XL, Su CY, Yang F (2016) FNN approximation-based active dynamic surface control for suppressing chatter in micro-milling with Piezo-actuators. *Ieee T Syst Man Cy-S* 1-14
- Pramanik A, Zhang LC, Arsecularatne JA (2007) An FEM investigation into the behavior of metal matrix composites: tool–particle interaction during orthogonal cutting. *Int J Mach Tool Manu* 47(10):1497–1506
- Zhou L, Huang ST, Wang D, Yu XL (2011) Finite element and experimental studies of the cutting process of SiCp/Al composites with PCD tools. *Int J Adv Manuf Technol* 52(5–8):619–626
- Zhu Y, Kishawy HA (2005) Influence of alumina particles on the mechanics of machining metal matrix composites. *Int J Mach Tool Manu* 45(4–5):389–398
- Kan Y, Liu ZG, Zhang SH, Zhang LW, Cheng M, Song HW (2014) Microstructure-based numerical simulation of the tensile behavior of SiCp/Al composites. *J Mater Eng Perform* 23(3):1069–1076
- Tursuna G, Weber U, Soppa E, Schmauder S (2006) The influence of transition phases on the damage behaviour of an Al/10vol.%SiC composite. *Comput Mater Sci* 37(1–2):119–133

**Publisher's note** Springer Nature remains neutral with regard to jurisdictional claims in published maps and institutional affiliations.